HTML ABSTRACT + LINKS

JOURNAL OF APPLIED PHYSICS VOLUME 95, NUMBER 3 1 FEBRUARY 2004

Modeling of magnetically enhanced capacitively coupled plasma sources: $Ar/C_4F_8/O_2$ discharges

Alex V. Vasenkov[a] and Mark J. Kushner[b]
Department of Electrical and Computer Engineering, University of Illinois, 1406 W. Green Street, Urbana, Illinois 61801

(Received 21 August 2003; accepted 21 October 2003)

Magnetically enhanced, capacitively coupled radio frequency plasma sources are finding continued use for etching of materials for microelectronics fabrication. MERIE (magnetically enhanced reactive ion etching) sources typically use magnetic fields of tens to hundreds of gauss parallel to the substrate to either increase the plasma density at a given pressure or to lower the operating pressure. The use of MERIEs for etching of dielectric materials, such as SiO_2, often involves the use of complex gas mixtures, such as $Ar/C_4F_8/O_2/CO$. In this paper results from a two-dimensional hybrid-fluid computational investigation of MERIE reactors operating in such mixtures are discussed. Fluxes and energy distributions for ions incident on the wafer are discussed for an industrially relevant geometry. The reduction in transverse electron mobility as the magnetic field increases produces a decrease in the sheath electric fields and a decrease in the dc bias (becoming more positive) at large magnetic fields thereby decreasing ion energies and increasing the angular spread of ions. These trends affect heavier ions more acutely than lighter ions. Subtle variations in the electrical geometrical layout of the reactor significantly affect the spatial uniformity of ion energy distributions. © *2004 American Institute of Physics.* [DOI: 10.1063/1.1633661]

I. INTRODUCTION

Magnetically enhanced capacitively coupled radio frequency (rf) plasma sources have been developed for the high plasma density etching and sputtering of materials for microelectronics fabrication; and are often called MERIE (magnetically enhanced reactive ion etching) reactors.[1–8] A typical MERIE reactor is a parallel plate device operating at tens to hundreds mTorr of gas pressure and of a few to tens of MHz excitation frequency. A static magnetic field, often rotating to smooth out inhomogeneities, is usually applied parallel to the electrodes with the goal of increasing the plasma density for a given power deposition by reducing the rate of loss of charged particles. The properties of magnetically enhanced capacitively coupled rf discharges sustained in Ar for an industrially relevant MERIE configuration were recently computationally investigated in Paper I.[9] Investigations into the operating characteristics of laboratory and commercial MERIE reactors[1–8,10–15] were also reviewed in Paper I.

In the study discussed in Paper I we found that as the magnetic field increased the dc bias decreased (became more positive), the plasma density became localized near the powered electrode, and there was a reversal of the electric field in the powered sheath. These trends, also predicted by Meyyappan,[16,17] were attributed to the reduction in cross magnetic field mobility of electrons resulting in a more resistive plasma and more current being carried by ions. The ranges of secondary electrons emitted by surfaces and accelerated by the sheaths were similarly decreased. The decrease in the dc bias contributes to a decrease in ion energies incident onto the substrate and a broadening of the ion angular distributions. As the magnetic field increases and electron mobility decreases the proportion of the rf cycle during which the sheath potential is at its minimum value increases and in some cases the electric field reverses. This trend contributes to decreasing the energy of the ion flux incident onto the substrate.

MERIE reactors are often used for the etching of dielectric materials using fluorocarbon gas mixtures.[18–23] For example, gas mixtures containing $Ar/c\text{-}C_4F_8/O_2/CO$ are used for the etching of SiO_2 in both MERIE and inductively coupled systems.[21–23] The purpose of these complex gas mixtures is to optimize the fluxes of material removing and polymerizing species to the substrate in order to obtain the preferential selectivity of etching a single material or to control the shape of the etch feature. In this paper, we report on a computational investigation of a MERIE sustained in $Ar/c\text{-}C_4F_8/O_2$ in an industrially relevant geometry. We found that similar to the pure argon discharge, the reduction in cross field electron mobility with increasing magnetic field produces a reduction in, and possibly reversal of, the electric field in the sheath, which reduces in energy and broadens in angle the ion flux incident on the wafer. Lighter ions are less sensitive to these trends as heavy ions are more likely to sample the sheath during its reversal. Subtle variations in the electrical boundaries of the reactor perturb the sheath and can produce radially nonuniform ion energy distributions incident onto the substrate. Ions of different masses have energy distributions with different radial dependencies as they respond to the perturbed sheath differently.

The model used in this study is discussed in Sec. II. Parametric results from our investigation of properties of

[a]Present address: CFD Research Corporation, 215 Wynn Drive, Huntsville, AL 35805; electronic mail: avv@cfdrc.com
[b]Author to whom all correspondence should be addressed; electronic-mail: mjk@uiuc.edu

Downloaded 08 Feb 2004 to 128.174.115.149. Redistribution subject to AIP license or copyright, see http://jap.aip.org/jap/copyright.jsp

$Ar/C_4F_8/O_2$ plasmas sustained in a MERIE are presented in Sec. III. Concluding remarks are in Sec. IV.

II. DESCRIPTION OF THE MODEL AND REACTION MECHANISM

The model used in this investigation is a fluid hydrodynamics simulation augmented by a Monte Carlo simulation (MCS) for secondary electrons. The model is the same as that used in Paper I where the simulation is described in detail. Briefly, continuity, momentum, and energy equations for neutrals and ions; continuity and energy equations for electrons and Poisson's equation for the electric potential are integrated in time to obtain a periodic steady state. The resulting electric fields and ion fluxes to surfaces are periodically transferred to the MCS where the transport of secondary electrons emitted from surfaces is addressed. Electron impact source functions and sources of secondary electron current obtained from the MCS are returned to the fluid model. The process is iterated to convergence. Following the last iteration, the converged electric fields and source functions for ions and neutrals are recorded as a function of position and phase in the rf cycle. With these values, the energy and angular distributions of ions and neutrals incident on the substrate are obtained using a heavy particle MCS module, and this module is also described in detail in Paper I.

A reaction mechanism was developed for plasmas sustained in gas mixtures initially consisting of arbitrary mole fractions of $Ar/c\text{-}C_4F_8/O_2/CO$. ($c\text{-}C_4F_8$ will be referred to as simply C_4F_8 herein.) This mechanism is described in detail in Ref. 24, and so will be only briefly discussed here. The limited electron impact cross-section data for the fluorocarbon species were collected and synthesized. Rate coefficients for gas phase chemistry were taken from independent studies in the literature or estimated from measurements for related species. In general, our approach was to include only the major species that influence plasma properties and reactant fluxes in order to minimize computational time. Since the computational time is less sensitive to the number of reactions, our mechanism is more exhaustive in that regard. Special care was taken to avoid so-called terminal species, which are produced but not consumed in the mechanism.

The electron impact cross sections for C_4F_8 were assembled using a combination of calculations,[25,26] mass spectrometry measurements,[27] and swarm (i.e., electron transport coefficient) analysis,[26] partially reviewed in Ref. 28. For example, time-of-flight mass spectrometry and laser photodetachment measurements indicate that the major negative ion formed by dissociative attachment to C_4F_8 is F^-. The branchings to other negative ions such as CF_3^-, $C_2F_3^-$, $C_3F_5^-$ were observed to be lower and they are not included in the model.[29–31] Vibrational excitation is the most important C_4F_8 inelastic process below about 10 eV. Consequently, the proportion of power that is channeled into vibrational excitations is significant. We developed analytical expressions for the C_4F_8 vibrational cross sections derived from swarm data so that these approximations could be more generally used.

Using mass spectrometry Toyoda *et al.*[32] and Jiao *et al.*[27] detected $C_2F_4^+$, $C_3F_5^+$, CF_3^+, CF^+, CF_2^+ as the major products of dissociative ionization of C_4F_8. The cross sections obtained by Toyoda *et al.* and Jiao *et al.* are consistent within the uncertainty of measurements and we chose to use Jiao's cross sections. The branching ratios for dissociative excitation of C_4F_8 into neutral fragments have not been studied in detail. Following modeling studies by Font *et al.*[26] and Rauf and Ventzek,[33] we assumed that

$$e + C_4F_8 \rightarrow C_2F_4 + C_2F_4 + e \tag{1}$$

is the major branching. This choice is consistent with data available for thermal and multiphoton dissociation of C_4F_8.[34,35] Mass spectrometry measurements for electron impact dissociation of C_4F_8 indicate branching to CF, CF_2, CF_3, C_3F_5 radicals.[32] These processes were not included in the mechanism since their cross sections are at least an order magnitude less than the total dissociation cross section at energies below about 50 eV.[26] Subsequent improvements to the model will include these branchings.

Due to the large ionization and neutral dissociation cross sections of C_4F_8 one can expect an abundance of C_2F_4 in C_4F_8 plasmas. The important electron impact C_2F_4 processes include elastic collisions, vibrational excitations, dissociation, and ionization. The cross sections of these processes were largely obtained from Refs. 36 and 37. Attachment was neglected since its branching is negligibly small.[36] Vibrational excitation cross sections of C_2F_4 were analytically represented using an approach similar to that used for C_4F_8.

Since CF_2 is the most likely product channel in C_2F_4 thermal dissociation reaction, we assumed that the major branching for electron impact dissociation of C_2F_4 is[34]

$$e + C_2F_4 \rightarrow CF_2 + CF_2 + e. \tag{2}$$

Another possible branching for C_2F_4 dissociation is

$$e + C_2F_4 \rightarrow CF_3 + CF + e. \tag{3}$$

Although this channel was neglected in our primary reaction mechanism, this is a likely reaction to refine the mechanism when additional experimental data became available.

A subset of the rate coefficients for neutral heavy particle reactions included in the mechanism was estimated. A major class of such rate constants is for deactivation of Ar* by fluorocarbon radicals. A second class is for associative reactions of CF_x radicals, $F + CF_x + M \rightarrow CF_{x+1} + M$. As these latter reactions are not terribly important at the pressure of interest (tens of mTorr) uncertainty in their values is not critical.

Ion–neutral reactions were classified as exothermic reactions, which occur independent of ion energy, and endothermic reactions that typically have energy defects of a few eV. The exothermic processes include the vast majority of reactions that occur at all locations in the plasma. The endothermic reactions mostly occur in the sheath, where ions are accelerated to energies in excess of the energy defect. Since for our conditions the sheath is at best mildly collisional, these latter processes were neglected. Ion–molecule reactions with many fluorocarbon feedstock gases and their fragments are often dissociative. For example Ar^+ has an ionization potential 15.8 eV sufficient to produce dissociative

Downloaded 08 Feb 2004 to 128.174.115.149. Redistribution subject to AIP license or copyright, see http://jap.aip.org/jap/copyright.jsp

ionization of C_4F_8 having a threshold of 11.5 eV, and most energetically allowed processes were included.

Electron–ion and ion–ion reactions were included in the mechanism as they determine the importance of volumetric loss of ions compared to diffusion to the walls. Since negative ions are generally lost only in the volume, these rates directly determine the negative ion density. The major class of estimated reactions here is ion–ion neutralization reactions as neither products of recombination nor reaction rates of these reactions are typically known. These reactions are fast as typical rate constants are $10^{-7}\ cm^3\ s^{-1}$. We estimated the rates of these reactions to be smaller for heavy ions and larger for lighter ions as the rate coefficient approximately scales as $\mu^{-0.5}$, where μ is the reduced mass of the colliding ions.[38,39] Another important class of estimated reactions is dissociative electron–ion recombination, whose rate coefficient is typically in the range of $10^{-7}/T_e^{1/2}\ cm^3\ s^{-1}$, where T_e is in eV.[40]

Validation of the reaction mechanism is discussed in detail in Ref. 24. An example of the validation process is shown in Fig. 1 for two systems. The first system is an inductively coupled plasma (ICP) sustained in C_4F_8 or Ar at 10 mTorr, flow rate of 40 sccm, and plasma volume of 2.4 l. Comparisons with experiment are shown for ion saturation current as a function of power in Fig. 1(a).[24,41] Quantitative agreement for both C_4F_8 and Ar are obtained, showing larger plasma densities in the less collisional Ar system. As the ion saturation current depends weakly on the mass of the ion, this comparison provides more secure validation of the total rate of ionization and losses than the details of reactions between species.

The second example of validation, shown in Fig. 1(b), is comparison of mass spectroscopic measurements from a capacitively coupled discharge sustained in Ar/C_4F_8 mixtures at 50 mTorr, 34 W, and 5 sccm (approximately 1 s residence time).[42] The fraction of light ions (C^+, CF^+, CF_3^+) increases with Ar dilution while the fraction of heavy ions ($C_2F_4^+$, $C_2F_5^+$, $C_3F_5^+$) decreases. (The balance of the ions is Ar^+.) These trends result from the larger fractional dissociation of the C_4F_8 with Ar dilution. For example, light ions are dominated by CF_3^+ at low Ar dilution and CF^+ at high Ar dilution.

To obtain agreement with experiments for densities of specific ions, some calibration of the reaction mechanism described in Ref. 24 was required. In particular, the rate coefficients for charge exchange of Ar^+ with CF_x radials and CF_2^+ with C_2F_4 were decreased by factors of 2–5. These adjustments, however, were highly dependent on the surface reaction mechanism. For example, the fraction of light ions are shown for two assumptions for the sticking coefficients of CF_x on all surfaces, 0.001 and 0.01. The ion fractions are, in some cases, more sensitive to uncertainties in these values of sticking coefficient than in the gas phase reaction coefficients.

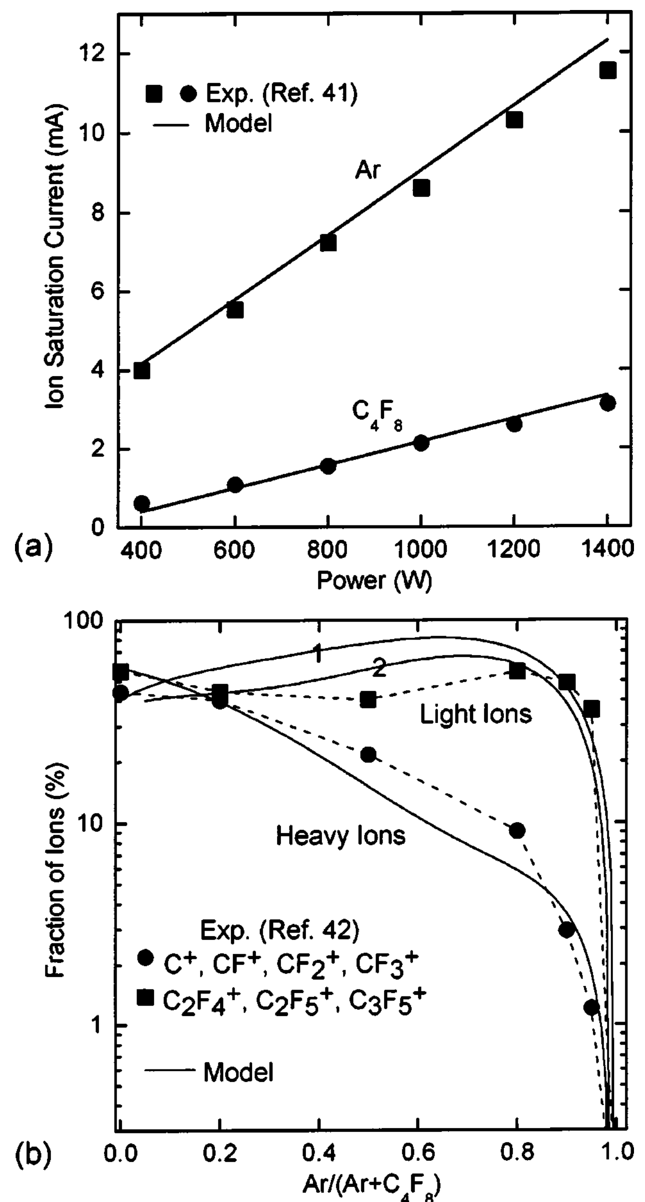

FIG. 1. Examples of validation of the reaction mechanism. (a) Ion saturation currents for Ar and C_4F_8 inductively couples plasmas (10 mTorr) as a function of power deposition. (Experimental results are from Ref. 41). (b) Fraction of light ions (C^+,CF^+,CF_2^+,CF_3^+) and heavy ions ($C_2F_4^+$,$C_2F_5^+$,$C_3F_5^+$) for a capacitively coupled discharge (50 mTorr, 34 W, 1 s residence time) as a function of Ar dilution in an Ar/C_4F_8 mixture. (Experimental results are from Ref. 42. The balance of ions are Ar^+.) Two results are shown for light ions where the sticking coefficients for CF_x radicals are (1) 0.001 and (2) 0.01.

III. PLASMA PROPERTIES IN MERIE REACTORS

The model reactor used in this study, shown schematically in Fig. 2, is patterned after plasma sources that are commercially available. The metal substrate is powered at 10

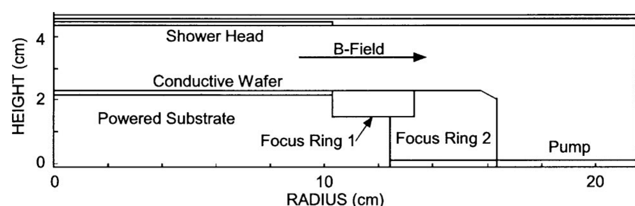

FIG. 2. Schematic of the MERIE geometry used in this study. The magnetic field is purely radial.

Downloaded 08 Feb 2004 to 128.174.115.149. Redistribution subject to AIP license or copyright, see http://jap.aip.org/jap/copyright.jsp

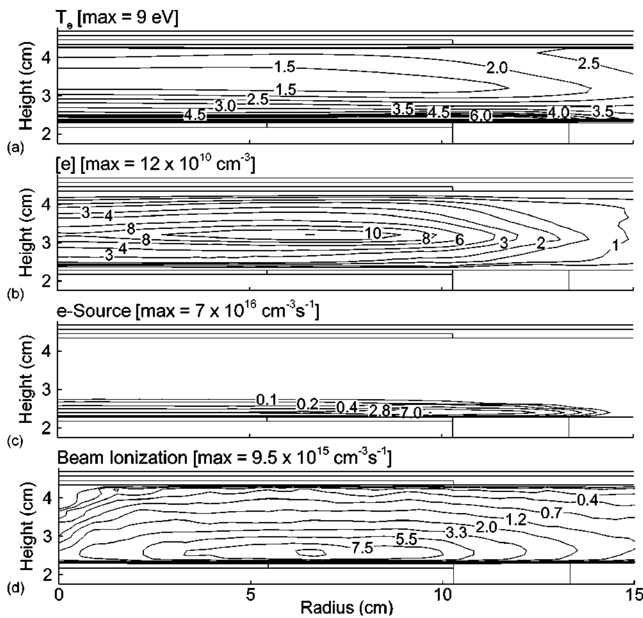

FIG. 3. Time averaged plasma parameters for the base case (1500 W, 40 mTorr with a flow rate of 215 sccm in the ratio of $Ar/C_4F_8/O_2 = 200/10/5$, 100 G). (a) Electron temperature, (b) electron density, (c) ionization source by bulk electrons, and (d) ionization source by beam electrons. Only the portion of the reactor between the electrodes is shown as the plasma does not significantly extend outwards. Ionization is dominated by beam electrons as the low mobility of bulk electrons constrains their extent.

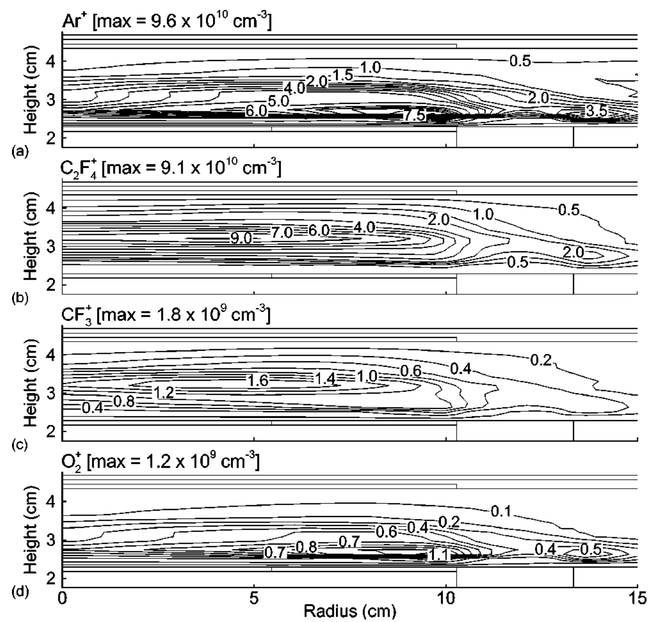

FIG. 4. Time averaged densities of selected ions for the base case (1500 W, 40 mTorr with a flow rate of 215 sccm in the ratio of $Ar/C_4F_8/O_2 = 200/10/5$, 100 G). (a) Ar^+, (b) $C_2F_4^+$, (c) CF_3^+ and (d) O_2^+. The spatial distributions of ions are determined by their ionization mechanisms. Ion formation mechanisms which are dominated by primary processes are localized near the substrate.

MHz through a blocking capacitor. A conductive Si wafer (σ=0.01/Ω cm), 20 cm in diameter, sits in electrical contact with the powered substrate which is surrounded by a Si ring (focus ring 1, $\epsilon/\epsilon_0 = 12.5$, $\sigma = 10^{-6}/\Omega$ cm) and dielectric focus ring (focus ring 2, $\epsilon/\epsilon_0 = 8.0$, $\sigma = 10^{-6}/\Omega$ cm). All other surfaces in the reactor are grounded metal including the showerhead, which extends to a radius of 10 cm, and the annular pump port. The base case operating conditions are 40 mTorr with a flow rate of 215 sccm in the ratio of $Ar/C_4F_8/O_2 = 200/10/5$, chosen as being similar to industrial processes, and 1500 W total power deposition. The rf bias amplitude is 512 V and the dc bias is -115 V. In this and other cases the rf amplitude was varied to obtain the desired power.

As this is a two-dimensional, cylindrically symmetric simulation, we are unable to address the true asymmetries and cross-wafer magnetic fields of industrial devices. As an approximation to these fields, we specified that the magnetic field be purely radial and parallel to the electrodes. As explained in Paper I, although this magnetic field is unphysical at $r = 0$, it is the configuration which best captures, within available computing resources, the behavior produced by asymmetric cross wafer magnetic fields.

Plasma parameters for the base case conditions are in Fig. 3 where the electron temperature (T_e), electron density ([e]), electron sources from electron impact by bulk electrons, and electron sources from electron impact by secondary electrons are shown. (The plasma is fairly well confined between the electrodes and does not appreciably extend into the volume above the pump port. Therefore only the region of the reactor directly above the substrate is shown in this and the following figures. This situation differs from the pure Ar discharge where there is considerable lateral extension of the plasma.) The density of a selection of positive ions (Ar^+, $C_2F_4^+$, CF_3^+, and O_2^+) are shown in Fig. 4 and the density of a selection of neutral radicals (CF_2, CF, F, and O) is shown in Fig. 5. Ion fluxes to the substrate as a function of radius are shown in Fig. 6. As in the case of the pure Ar (see Paper

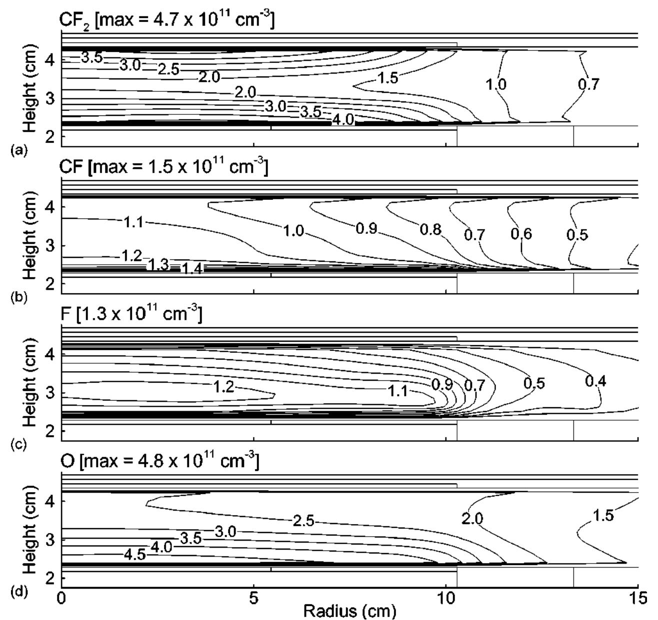

FIG. 5. Time averaged densities of selected radicals for the base case (1500 W, 40 mTorr with a flow rate of 215 sccm in the ratio of $Ar/C_4F_8/O_2 = 200/10/5$, 100 G). (a) CF_2, (b) CF, (c) F, and (d) O. The spatial distributions of radicals is determined by whether their formation is dominated by wall or bulk reactions.

Downloaded 08 Feb 2004 to 128.174.115.149. Redistribution subject to AIP license or copyright, see http://jap.aip.org/jap/copyright.jsp

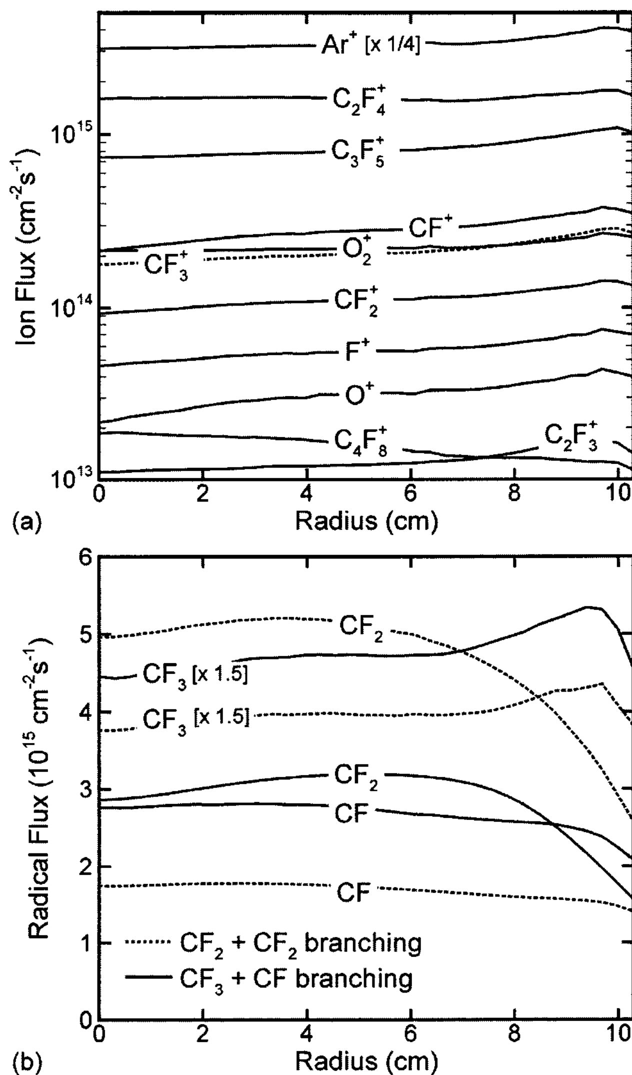

FIG. 6. Ion fluxes to the substrate as a function of radius for the base case conditions (1500 W, 40 mTorr with a flow rate of 215 sccm in the ratio of $Ar/C_4F_8/O_2=200/10/5$, 100 G). (a) Ion fluxes and (b) radical fluxes. Results for two branchings for electron impact dissociation of C_2F_4 are shown for the radical fluxes.

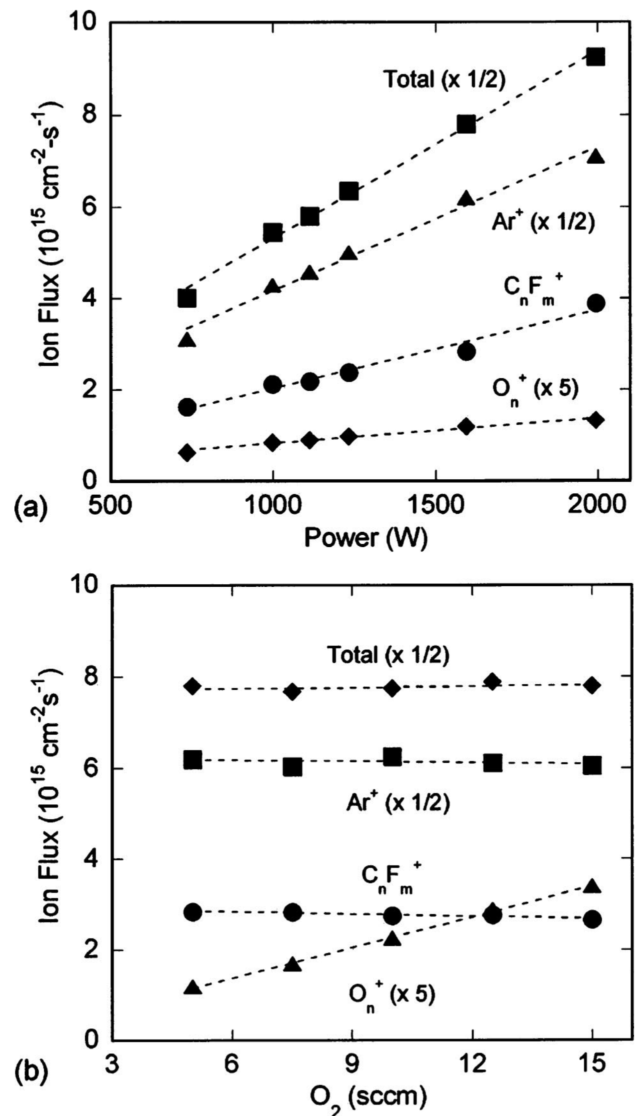

FIG. 7. Ion fluxes to the center of the wafer as a function of (a) power deposition and (b) O_2 flow rate. The conditions are otherwise the same as the base case. Over the range of powers investigated, the relative mole fractions of ions do not appreciably change.

I), T_e peaks in and near the sheath with little extension into the bulk plasma. This is a consequence of the low cross field mobility of electrons in the axial direction in the 100 G magnetic field. (The Larmor radius of electrons for these conditions is ≈0.6 mm.) The electron mobility is unhindered parallel to the magnetic field, and so the region of high electron temperature extends laterally across the focus rings. The electron temperature actually peaks above the focus rings, a situation that will be discussed in the following.

Since T_e is highly peaked toward the substrate, the electron ionization source by bulk electrons is also highly confined near the substrate. There is little ionization by bulk electrons in the middle of the gap. This differs markedly from the argon only case where significant bulk ionization extended into the gap. The difference here is that excited states of argon, principally Ar(4s), are less likely to be excited and are quenched by collisions with molecular species. In the argon only case these states are long lived, thereby providing for multistep ionization deep into the gap. The ionization by beam, sheath accelerated electrons extends across the gap and dominates the source of ionization. The initial electron beam energy is, on average, $V_p - V_{dc}$ [(time averaged plasma potential)—(dc bias)] which, in this case, is 190 eV. The maximum beam energy (peak of the cathodic cycle) is 575 eV. These energies provide sufficient penetration distance and large enough Larmor radius to cross the gap.

The major positive ions have densities of $1\times10^{11}\,cm^{-3}$ (see Fig. 4). The spatial distribution of ions in part indicates their formation mechanisms. (In this discussion, primary ionization processes refer to direct electron impact on feedstock gases. Secondary ionization processes refer to electron impact on dissociation products of feedstock gases, by charge exchange or Penning processes.) Ar^+, having the highest ionization potential, has only primary ionization processes and is rapidly depleted by charge exchange. As a result, Ar^+ has peak densities near the sheath where the

Downloaded 08 Feb 2004 to 128.174.115.149. Redistribution subject to AIP license or copyright, see http://jap.aip.org/jap/copyright.jsp

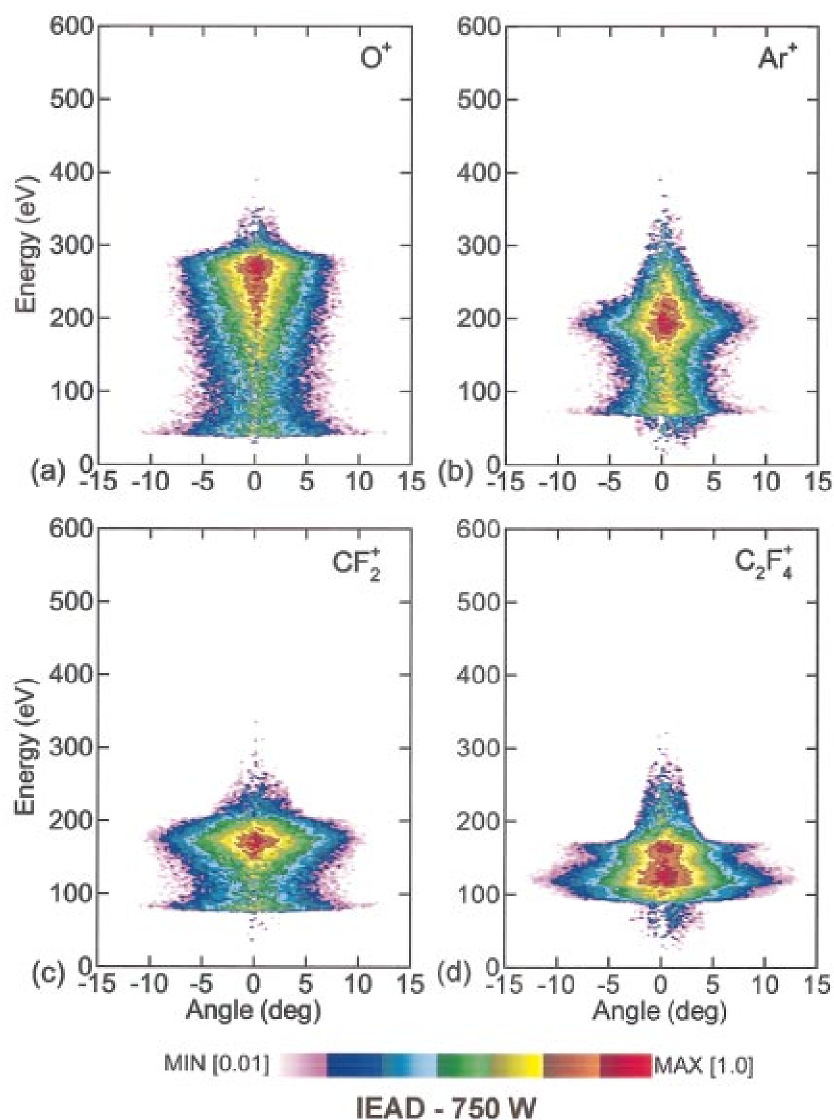

FIG. 8. (Color) Ion energy and angular distributions incident on the outer 4 cm radius of the wafer for 750 W but otherwise the base case conditions. (a) O^+, (b) Ar^+, (c) CF_2^+, and (d) $C_2F_4^+$. The dynamic range of the plots is 2 decades on a log-scale.

electron temperature and beam sources are largest. $C_2F_4^+$ is formed by both primary (electron impact on C_4F_8) and secondary processes (electron impact on C_2F_4, and charge exchange from Ar^+, O^+, O_2^+ and smaller CF_n^+ fragments to C_2F_4). Its density is therefore more distributed in the reactor, though skewed toward the region of highest ionization sources. CF_3^+ is mostly formed only by secondary ionization processes as its rate of production by dissociative ionization of C_4F_8 is small. The CF_3^+ density therefore peaks close to the maximum in the plasma potential. O_2^+, similar to Ar^+, is formed dominantly by primary processes with a smaller contribution of secondary processes (charge exchange from Ar^+), while also being rapidly depleted by charge exchange. O_2^+ therefore also peaks near the maximum in the ionization sources.

The spatial distribution of radical densities shown in Fig. 5 also reflects their origins. CF_2 has maxima near top and bottom electrodes, which in part results from the large flux of CF_2^+ that is neutralized on surfaces and returns as CF_2. The CF_2 has smaller sources in the bulk as a consequence of the lower rate of dissociation of C_2F_4. CF is primarily formed by secondary processes which dominate in the bulk and which also dominate over neutralization of its ion fluxes on surfaces. F atoms are formed in large part by direct electron impact dissociation of fluorocarbons whose branching ratios favor higher energy electrons. We therefore find its sources dominated by the beam electrons and its density is more distributed. O atoms are formed in large part by dissociative excitation of O_2, which peaks near the lower electrode and by neutralization of O^+ fluxes.

The fluxes of the major ions to the substrate as a function of radius are shown in Fig. 6(a) for the base case conditions. The ion fluxes are dominated by Ar^+ due to both its large mole fraction in the gas feed and by the peak in the Ar^+ density being in close proximity to the substrate. The fluorocarbon ion fluxes are dominated by the heavier ions. The ion fluxes are fairly uniform with a tendency toward being edge high, though little attempt was made to optimize uniformities in this study. Since the uniformities of ion fluxes are sensitive functions of geometry and materials used in construction of the reactor, we will not comment generally on them other than for brief discussion at the end of this section.

Downloaded 08 Feb 2004 to 128.174.115.149. Redistribution subject to AIP license or copyright, see http://jap.aip.org/jap/copyright.jsp

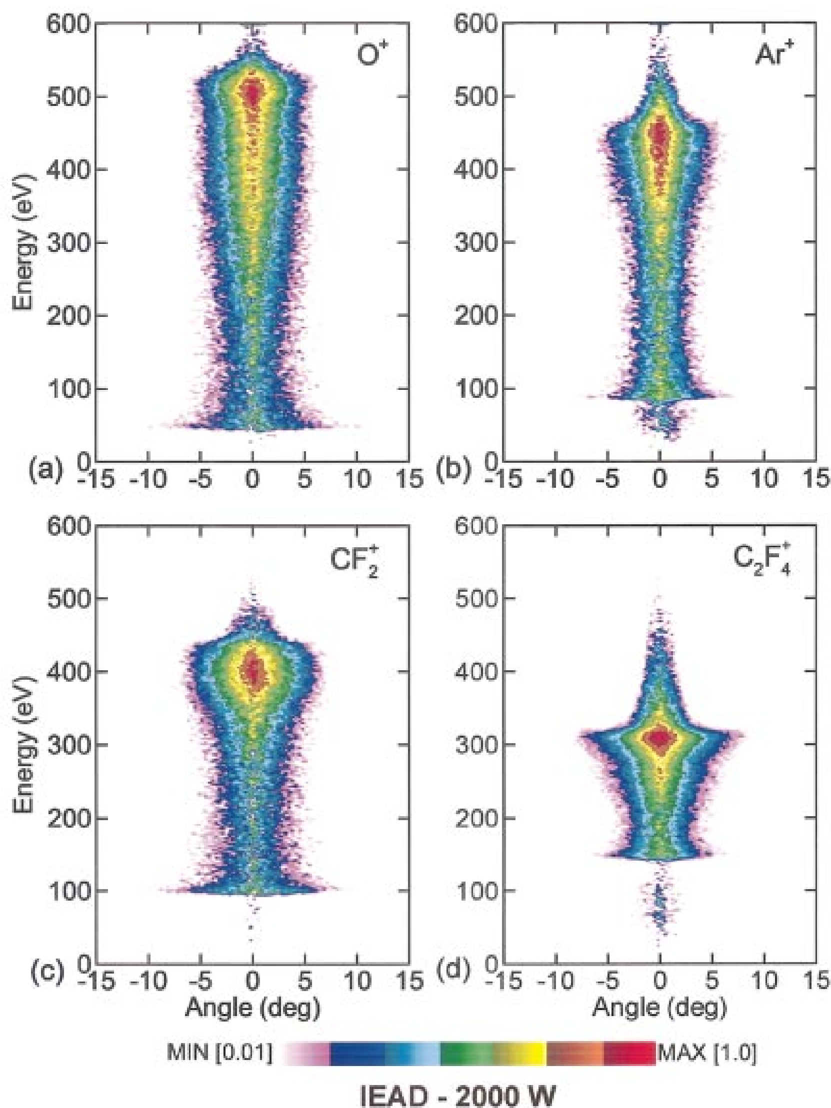

FIG. 9. (Color) Ion energy and angular distributions incident on the outer 4 cm radius of the wafer for 2000 W but otherwise the base case conditions. (a) O^+, (b) Ar^+, (c) CF_2^+, and (d) $C_2F_4^+$. The dynamic range of the plots is 2 decades on a log-scale.

$C_4F_8^+$ is not believed to be a stable product of electron impact ionization of c-C_4F_8 as it is likely to predissociate into smaller fragments in the absence of collisional stabilization.[28] A form of stable $C_4F_8^+$ can, however, be formed by charge exchange from CO^+, O^+ and O_2^+ to 2-C_4F_8.[43] Since the ionization potential of $C_4F_8^+$ is among the lowest of all positive ions in the mechanism it is nearly immune from depletion by charge exchange. With its low mobility, it is also slow to diffuse or drift out of the plasma, and so any significant production $C_4F_8^+$ is likely to result in its accumulation in the discharge. As a worst case analysis, we included the charge exchange reactions from CO^+, O^+ and O_2^+ to c-C_4F_8 using the values measured for 2-C_4F_8.[43] Even in this worst case, the flux and density of $C_4F_8^+$ is a small fraction of the total, as shown in Fig. 6(a). Including charge exchange to form $C_4F_8^+$ decreases the ion fluxes of O_2^+ by $\approx$10% but otherwise does not significantly perturb the system.

The major branching for electron dissociative ionization we used for C_4F_8 is $C_2F_4+C_2F_4^+$ with minor branchings to $C_3F_5^+$, CF^+, CF_2^+, and CF_3^+. The major dissociative electronic excitation branching of C_2F_4 is to CF_2+CF_2. The former branchings are based on experimental measurements[27] whereas the latter is an assumption also used in other modeling efforts.[26,33] The final disposition of ion and radical fluxes to the substrate is sensitive to both of these branchings and the disposition of product ions by charge exchange. For example, a sensitivity analysis was performed where the branching ratio for dissociative excitation of C_2F_4 was changed from CF_2+CF_2 to $CF+CF_3$, and all energetically allowed charge exchange reactions of fluorocarbon radicals with Ar^+ were included, which required addition of charge exchange with CF_2 and CF. The rate coefficients for the added reactions are the same as for charge exchange of Ar^+ with CF_3 to form CF_3^+, $k=7\times10^{-10}\,cm^3\,s^{-1}$.[44] Moderate increases (5%–15%) in the fluxes of CF^+, CF_2^+, and CF_3^+ were produced. Fluxes of the neutral radicals CF and CF_3 were significantly increased while that for CF_2 decreased [see Fig. 6(b)].

The ion fluxes at the center of the wafer as a function of power deposition and O_2 flow rate are shown in Fig. 7. The relative fluxes of ions do not appreciably vary over the range of powers investigated, with their absolute values increasing nearly linearly with power. With increasing flow rate of O_2,

Downloaded 08 Feb 2004 to 128.174.115.149. Redistribution subject to AIP license or copyright, see http://jap.aip.org/jap/copyright.jsp

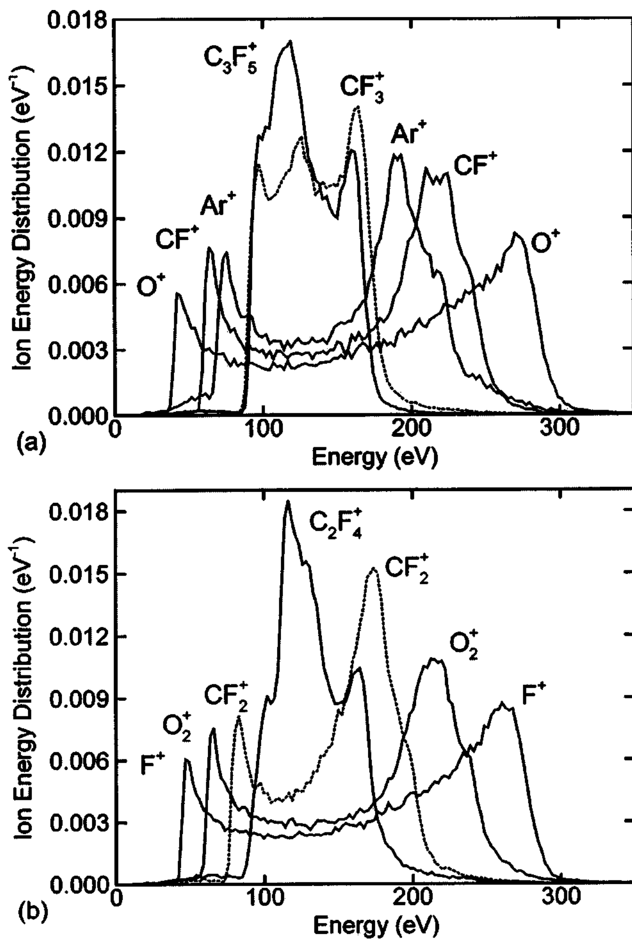

FIG. 10. Ion energy distributions, integrated over angle, incident on the outer 4 cm radius of the wafer for 750 W but otherwise the base case conditions for a selection of light and heavy ions. (a) O^+, CF^+, Ar^+, CF_3^+, and $C_3F_5^+$; and (b) F^+, O_2^+, CF_2^+, and $C_2F_4^+$.

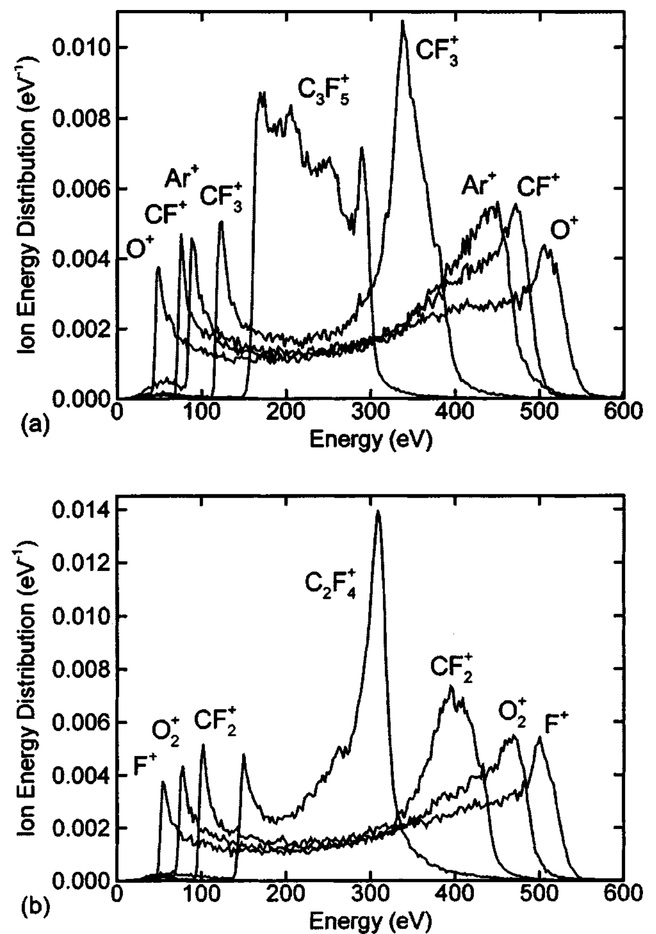

FIG. 11. Ion energy distributions, integrated over angle, incident on the outer 4 cm radius of the wafer for 2000 W but otherwise the base case conditions for a selection of light and heavy ions. (a) O^+, CF^+, Ar^+, CF_3^+, and $C_3F_5^+$; and (b) F^+, O_2^+, CF_2^+, and $C_2F_4^+$.

there are small decreases in the fluxes of other ion fluxes while those for O_2 increase. Even for the largest flow rate of O_2 investigated here, the total mole fraction is still small (<8%). These relatively low O_2 mole fractions, choices based on industrially used gas mixtures, are used to minimize the amount of erosion of the photoresist mask and depletion of polymer layers by oxygen radicals.

The ion energy and angular distributions (IEADs) of a selection of light and heavy ions are shown in Fig. 8 for 750 W and in Fig. 9 for 2000 W but otherwise for the base case conditions. The ions are incident on the outer 4 cm of the wafer. The ion energy distributions (IEDs) integrated over angle for a wider selection of ions are shown in Figs. 10 and 11. The rf voltage amplitude was varied to obtain the cited powers. The rf voltage amplitude was 409 V (with a dc bias of −69 V) for 750 W and 582 V (dc bias −141 V) for 2000 W. The IEADs have the characteristic two-peak distribution commonly found in rf biased systems.[45,46] Heavier ions have narrow IEADs in energy and broader IEADs in angle, a consequence of their longer crossing time across the sheath and their likelihood for being more collisional. The IEADs differ from those obtained in conventional RIE systems primarily at lower energies. Note that for most ions, there is a "foot" to the IEAD extending to lower energies.

As discussed in Paper I, the decrease in electron mobility due to the transverse magnetic field results in a more resistive bulk plasma and a thickening of the sheath. At sufficiently large magnetic fields (>150 G) the mobility of the lighter positive ions may exceed the transverse mobility of electrons. The end result is that the time during the rf cycle that the sheath at the powered electrode is at its minimum potential, during which electron current is collected, is progressively longer as the magnetic field increases. These trends are shown in Fig. 12 where the plasma potential as a function of height (radius of 5 cm) is plotted at different times during the rf cycle for B fields of 50, 100, and 250 G. At sufficiently large magnetic fields, the sheath switches from being electron repelling and positive ion attracting during the cathodic part of the cycle to electron attracting and positive ion repelling during the anodic part of the cycle. In conventional RIE systems, the sheath is usually positive ion attracting (or at best not repelling) during the entire rf period. With the reduced electron mobility at high magnetic fields, insufficient electron current is collected with the conventional sheath structure. The reversal of the sheath occurs while the plasma becomes more resistive and more voltage is dropped across the bulk plasma. The smaller electric fields in the sheaths or, at higher magnetic fields, the reversal of elec-

Downloaded 08 Feb 2004 to 128.174.115.149. Redistribution subject to AIP license or copyright, see http://jap.aip.org/jap/copyright.jsp

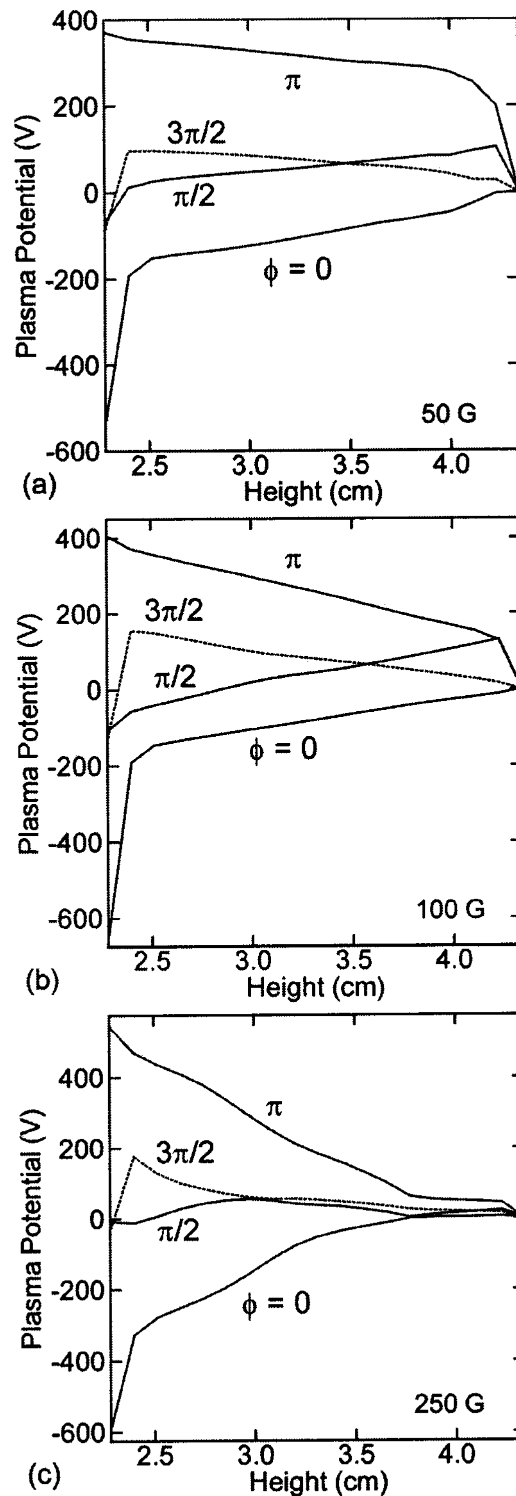

FIG. 12. Plasma potential as a function of height at a radius of 5 cm at different phases during the rf cycle. (a) 50 G, (b) 100 G, and (c) 250 G. The conditions are otherwise the same as the base case (1500 W, 40 mTorr with a flow rate of 215 sccm in the ratio of $Ar/C_4F_8/O_2=200/10/5$). With increasing magnetic field, the plasma becomes more resistive and the electric field in the sheath above the powered electric decreases or reverses.

tric fields in the sheaths, reduce the ion energies striking the substrates. The end results are IEADs with large, low energy components having broad angular distributions.

The IEADs of heavier ions at lower powers are more susceptible to the flattening or reversal of the sheaths. Comparing the IEADs for 750 and 2000 W, we find a proportionally larger low energy component at the lower power for the heavier ions. We found that the electric field in the bulk plasma is nearly independent of power for a given magnetic field. Therefore, at lower powers a larger fraction of the applied voltage is dropped across the bulk plasma. As the power and rf voltage are increased, the fraction of the applied voltage which is dropped across the sheath increases thereby enabling more efficient ion acceleration. This occurs while the fraction of the rf cycle when the sheath is at its minimum value (or reversed) to collect electron current also decreases, thereby reducing the propensity for deceleration and broadening of the IEAD.

These trends are further illustrated by the IEADs shown in Fig. 13 for O^+ (a light ion) and $C_2F_4^+$ (a heavy ion) for magnetic fields of 100, 200, and 250 G. The rf voltage amplitude and dc bias for these cases are [512 V, −116 V]; [538 V, −25 V]; and [569 V, −21 V] respectively. As discussed in Paper I, as the magnetic field increases, the dc bias decreases (becomes more positive) as the mobility of the electrons decreases relative to that of the ions and the plasma is more confined above the electrodes. On the other hand, the rf voltage amplitude increases as the plasma becomes more resistive. A measure of the average ion energy for heavy ions is the difference between the time averaged plasma potential and the dc substrate potential, $V_p - V_{dc}$. In spite of the rf amplitude increasing with increasing B field, the decrease in dc bias (more positive) and the decrease (or reversal) of the sheath electric fields produce values of $V_p - V_{dc}$ of 189, 109, and 93 V for the 100, 200 and 250 G cases. As a consequence, the IEADs both decrease in energy and broaden in angle. The effects are particularly severe for the heavier ions. At least a portion of the ion flux for lighter ions is able to transition through the sheath during that portion of the rf cycle when the electric field in the sheath is not at its minimum value (or reversed). All heavy ions, however, experience the reversal of the electric fields in the sheath as their residence times in the sheath are many rf cycles. As a result, their IEADs broaden more severely.

Although the intent of this study was not to optimize geometries for uniformity, a flaw in our initial reactor design provides insights to the potential sources of nonuniformities in IEADs. As the rates of surface reactions for endothermic processes are sensitive to the energy of the incident ions,[47] nonuniformities in the IEADs as well as the magnitude of the fluxes are of concern in optimizing etch uniformity. For example, the IEDs for a light (O^+) and heavy ($C_2F_4^+$) ion are shown in Fig. 14(a) for ions incident at the center of the wafer (inner 3.3 cm radius) and on the edge of the wafer (outer 1.8 cm radius) for the base case conditions. In each case, the IED is broadened at the edge of the wafer, with more emphasis on the higher energies for the light ion and lower energies for the heavy ions.

The source of these nonuniformities in the IEDs can be traced to the proximity of the electrical ground plane under the focus rings surrounding the substrate and wafer. The electric potential at the peak of the anodic and cathodic phases of the rf cycle are shown in Fig. 15(a). In this design, the ground plane extends under the focus rings, which forces

Downloaded 08 Feb 2004 to 128.174.115.149. Redistribution subject to AIP license or copyright, see http://jap.aip.org/jap/copyright.jsp

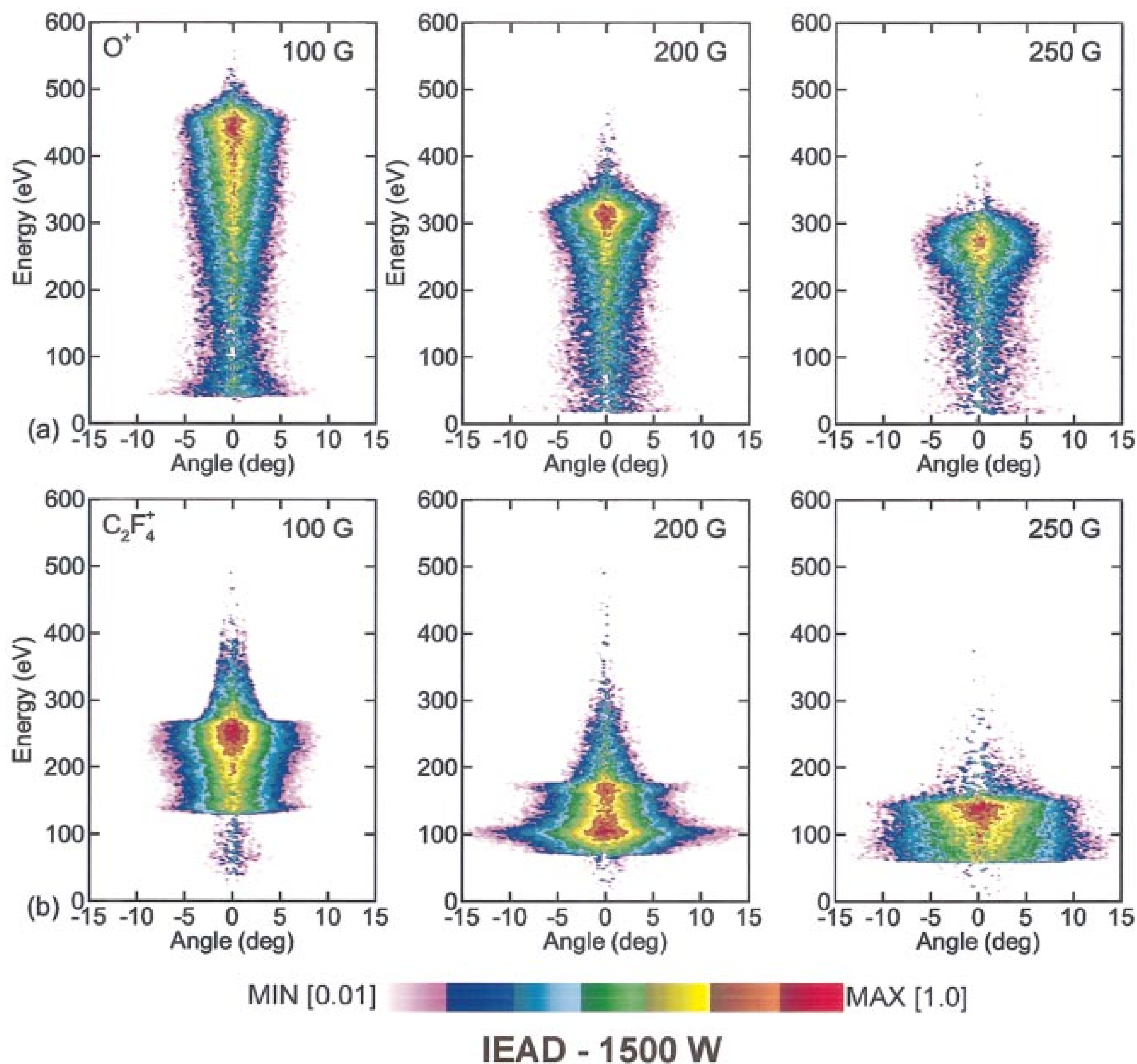

FIG. 13. (Color) Ion energy and angular distributions for magnetic fields of 100, 200, and 250 G for (a) O^+ and (b) $C_2F_4^+$. The conditions are otherwise the same as the base case (1500 W, 40 mTorr with a flow rate of 215 sccm in the ratio of $Ar/C_4F_8/O_2=200/10/5$). The IEADs of the heavier ions are more susceptible to energy degradation and broadening as the magnetic field increases.

the applied potential to be largely dissipated through the dielectrics. As the dielectric charge and discharge during the rf cycle the potential contours are warped at the edge of the wafer. The end result is a region of larger time averaged electric field having a thicker sheath in the vicinity of the edge of the wafer. For lighter ions, their traversal time through the thicker sheath is sufficiently short that they primarily gain in energy. For heavier ions, the longer residence time in the thicker sheath provides for more deceleration by the sheath reversal, creating a larger low-energy peak in the IED, which is also broadened in energy. The larger sheath electric field produced by the fringing potential is also responsible for the local peak in electron temperature.

This flaw in the design was corrected by replacing the electrically grounded metal below the focus rings with a metal in electrical contact with the powered electrode. The potential under the focus rings is therefore driven with the same voltage as the substrate, which stretches the potential contours in the radial direction, as shown in Fig. 15(b). The enhancements in the electric field and sheath at the edge of the wafer are reduced, resulting in a more uniform sheath across the wafer. The IEDs for this design at the center and edge of the wafer for both light and heavy ions are essentially the same, as shown in Fig. 14(b). This configuration does, however, produce a smaller rf amplitude and dc bias (455 and −49 V) and so the IEDs, though more uniform, are lower in energy.

IV. CONCLUDING REMARKS

The properties of an industrially relevant MERIE plasma source sustained in $Ar/C_4F_8/O_2$ gas mixtures have been

Downloaded 08 Feb 2004 to 128.174.115.149. Redistribution subject to AIP license or copyright, see http://jap.aip.org/jap/copyright.jsp

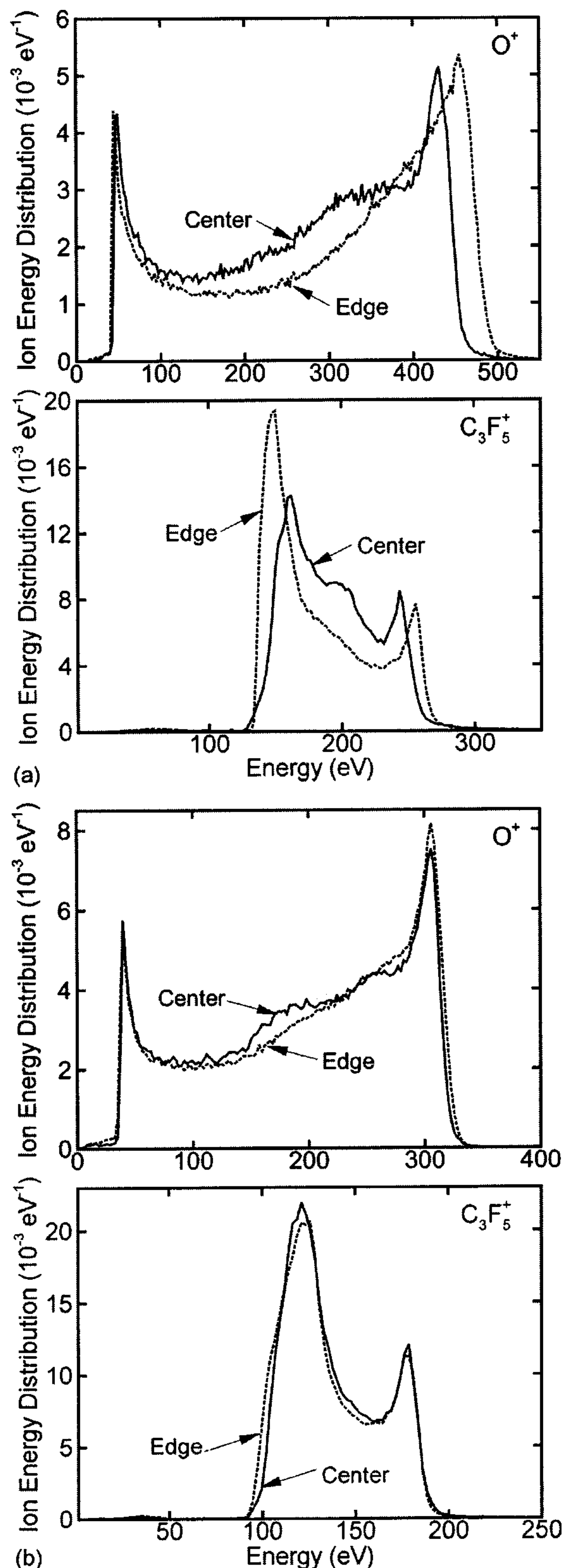

FIG. 14. Ion energy distributions for O^+ and $C_3F_5^+$ incident on the center (inner 3.3 cm radius) and edge (outer 1.8 cm radius) of the wafer for the base case conditions (1500 W, 40 mTorr with a flow rate of 215 sccm in the ratio of $Ar/C_4F_8/O_2 = 200/10/5$, 100 G). (a) With the electrical ground plane under the focus rings and (b) with the powered electrode extended under the focus rings. The disparity between center and edge with the ground plane under the focus rings is attributed to deformation of the sheath by the proximity of the ground plane.

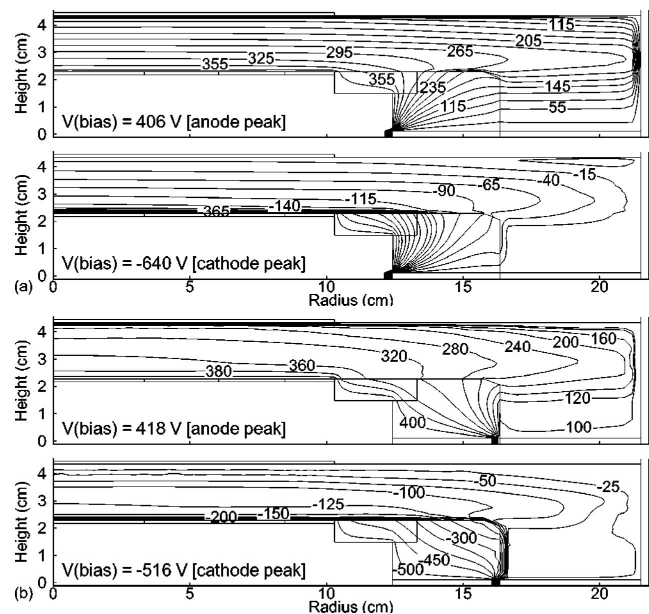

FIG. 15. Electric potential at the peak of the anodic and cathodic phases of the rf cycle for the base case conditions for (a) with the electrical ground plane under the focus rings and (b) with the powered electrode extended under the focus rings. The rf amplitude and dc bias for the grounded case are 525 and −115 V. For the powered case the values are 465 and −49 V.

computationally investigated using results from a two-dimensional plasma transport model. Trends observed for pure argon discharges generally apply to the more complex gas mixtures; decreasing dc bias (more positive), localization of plasma density near the powered electrode, and reversal of the electric field in the powered sheath with increasing magnetic field. These trends are attributed to the reduction in cross field mobility of electrons resulting in a more resistive plasma and more current being carried by ions. The more complex gas mixture has a larger variety of ions incident on the substrate having nearly an order of magnitude difference in molecular weight. The decrease (or reversal) of the sheath electric fields during larger fractions of the rf cycle as the magnetic field increases generally degrade the IEAD in energy and broaden the angular spread. Heavier ions are more sensitive to the decrease (or reversal) of the sheath electric fields as their residence time in the sheath is longer. Therefore heavy ions sample the weak or retarding sheath for proportionately longer times. Nonuniformities in the IEADs as a function of position on the wafer can be traced to details of the design of the reactor. In particular the placement of the electrical ground plane can perturb sheath properties, both thickness and potential drop. Since ions of different mass respond to these perturbations differently, the radial dependencies of their IEADs are also different.

ACKNOWLEDGMENTS

This work was supported by the National Science Foundation (CTS99-74962 CTS03-15353), the Semiconductor Research Corp., CFD Research Corp. and SEMATECH. The author thanks Dr. Vivek Bakshi of SEMATECH and Dr. William Dostalik of Texas Instruments for their helpful comments and assistance.

Downloaded 08 Feb 2004 to 128.174.115.149. Redistribution subject to AIP license or copyright, see http://jap.aip.org/jap/copyright.jsp

[1] R. A. Lindley, C. H. Bjorkman, H. Shan, K.-H. Ke, K. Doan, R. R. Mett, and M. Welch, J. Vac. Sci. Technol. A **16**, 1600 (1998).
[2] K. E. Davies, M. Gross, and C. M. Horwitz, J. Vac. Sci. Technol. A **11**, 2752 (1993).
[3] M. J. Buie, J. T. P. Pender, and P. L. G. Ventzek, Jpn. J. Appl. Phys., Part 1 **36**, 4838 (1997).
[4] P. Berruyer, F. Vinet, H. Feldis, R. Blanc, M. Lerme, Y. Morand, and T. Poiroux, J. Vac. Sci. Technol. A **16**, 1604 (1998).
[5] C. T. Gabriel, J. Vac. Sci. Technol. B **20**, 1542 (2002).
[6] C. O. Jung, K. K. Chi, B. G. Hwang, J. T. Moon, M. Y. Lee, and J. G. Lee, Thin Solid Films **341**, 112 (1999).
[7] M. J. Buie, J. T. P. Pender, and M. Dahimene, J. Vac. Sci. Technol. A **16**, 1464 (1998).
[8] A. P. Paranjipe, M. M. Moslehi, and C. J. Davis, J. Vac. Sci. Technol. A **10**, 1140 (1992).
[9] M. J. Kushner, J. Appl. Phys. **94**, 1436 (2003).
[10] G. Y. Yeom, J. A. Thornton, and M. J. Kushner, J. Appl. Phys. **65**, 3816 (1989).
[11] G. Y. Yeom, J. A. Thornton, and M. J. Kushner, J. Appl. Phys. **65**, 3825 (1989).
[12] D. A. W. Hutchinson, M. M. Turner, R. A. Doyle, and M. B. Hopkins, IEEE Trans. Plasma Sci. **23**, 636 (1995).
[13] S. V. Avtaeva, M. Z. Manytbekov, and D. K. Otorbaev, J. Phys. D **30**, 3000 (1997).
[14] J.-C. Park and B. Kang, IEEE Trans. Plasma Sci. **25**, 499 (1997).
[15] M. A. Lieberman, A. J. Lichtenberg, and S. E. Sava, IEEE Trans. Plasma Sci. **19**, 189 (1991).
[16] M. Meyyappan, J. Appl. Phys. **71**, 2574 (1992).
[17] M. Meyyappan and T. R. Govindan, J. Vac. Sci. Technol. A **10**, 1344 (1992).
[18] K. Miyata, M. Hori, and T. Goto, J. Vac. Sci. Technol. A **15**, 568 (1997).
[19] J.-P. Booth, Plasma Sources Sci. Technol. **8**, 249 (1999).
[20] K. Sasaki, Y. Kawai, C. Suzuki, and K. Kadota, J. Appl. Phys. **83**, 7482 (1998).
[21] X. Li, L. Ling, X. Hua, M. Fukasawa, and G. S. Oehrlein, J. Vac. Sci. Technol. A **21**, 284 (2003).
[22] M. Matsui, T. Tatsumi, and M. Sekine, J. Vac. Sci. Technol. A **19**, 2089 (2001).
[23] M. Matsui, T. Tatsumi, and M. Sekine, J. Vac. Sci. Technol. A **19**, 1282 (2001).
[24] A. V. Vasenkov, X. Li, G. S. Oehrlein, and M. J. Kushner, J. Vac. Sci. Technol. A (to be published).
[25] C. Winstead and V. McKoy, J. Chem. Phys. **114**, 7407 (2001).
[26] G. I. Font, W. L. Morgan, and G. Mennenga, J. Appl. Phys. **91**, 3530 (2002).
[27] C. Q. Jiao, A. Garscadden, and P. D. Haaland, Chem. Phys. Lett. **297**, 121 (1998).
[28] L. G. Christophorou and J. K. Olthoff, J. Phys. Chem. Ref. Data **30**, 449 (2001).
[29] P. W. Harland and J. L. Franklin, J. Chem. Phys. **61**, 1621 (1974).
[30] I. Sauers, L. G. Christophorou, and J. G. Carter, J. Chem. Phys. **71**, 3016 (1979).
[31] J. E. Sanabia, G. D. Cooper, J. A. Tossell, and J. H. Moore, J. Chem. Phys. **108**, 389 (1998).
[32] H. Toyoda, M. Iio, and H. Sugai, Jpn. J. Appl. Phys., Part 1 **36**, 3730 (1997).
[33] S. Rauf and P. L. G. Ventzek, J. Vac. Sci. Technol. A **20**, 14 (2002).
[34] S. H. Bauer and S. Javanovic, Int. J. Chem. Kinet. **30**, 171 (1998).
[35] A. Yokoyama, K. Yokoyama, and G. Fujisawa, Chem. Phys. Lett. **237**, 106 (1995).
[36] K. Yoshida, S. Goto, H. Tagashira, C. Winstead, B. V. McKoy, and W. L. Morgan, J. Appl. Phys. **91**, 2637 (2002).
[37] C. Winstead and V. McKoy, J. Chem. Phys. **116**, 1380 (2002).
[38] J. T. Moseley, R. E. Olson, and J. R. Peterson, Case Stud. At. Phys. **5**, 1 (1975).
[39] A. P. Hickman, J. Chem. Phys. **70**, 4872 (1979).
[40] M. A. Biondi, in *Principles of Laser Plasmas*, edited by G. Bekefi (Wiley, New York, 1976).
[41] X. Li, L. Ling, X. Hua, G. S. Oehrlein, Y. Wang, A. V. Vasenkov, and M. J. Kushner, J. Vac. Sci. Technol. A (submitted).
[42] Y. Hirose, I. Ishikawa, S. Sasaki, K. Nakeskei, Y. Saito, and S. Suganomata, Jpn. J. Appl. Phys., Part 1 **37**, 5730 (1998).
[43] G. K. Jarvis, C. A. Mayhew, and R. P. Tuckett, J. Phys. Chem. **100**, 17166 (1996).
[44] Estimated by analogy to CF_4. See E. R. Fisher, M. E. Weber, and P. B. Armentrout, J. Chem. Phys. **92**, 2296 (1990).
[45] M. A. Sobolewski, Y. Wang, and A. Goyette, J. Appl. Phys. **91**, 6303 (2002).
[46] N. Mizutani and T. Hayashi, J. Vac. Sci. Technol. A **19**, 1298 (2001).
[47] G. S. Oehrlein, M. F. Doemling, B. E. E. Kastenmeier, P. J. Matsuo, N. R. Rueger, M. Schaepkens, and T. E. F. M. Standaert, IBM J. Res. Dev. **42**, 181 (1999).

Downloaded 08 Feb 2004 to 128.174.115.149. Redistribution subject to AIP license or copyright, see http://jap.aip.org/jap/copyright.jsp